Paper No.
11537

NACE INTERNATIONAL CORROSION 2018 Conference & Expo

Effect of Corrosion Inhibitor Alkyl Tail Length on the Electrochemical Process Underlying CO_2 Corrosion of Mild Steel

J.M. Domínguez Olivo, D. Young, B. Brown, S. Nesic
Institute for Corrosion and Multiphase Technology
Department of Chemical & Biomolecular Engineering
Ohio University
Athens, OH 45701

ABSTRACT

Surfactant-type organic corrosion inhibitors are widely used in the oil and gas industry to mitigate internal pipeline corrosion. Their molecular structure is comprised of a polar head group and a non-polar alkyl tail, with different lengths. Despite many studies qualitatively associating the alkyl tail length to the corrosion mitigation efficiency, there is are no systematic studies and no clear mechanistic explanation in the literature about how the alkyl tail length affects the corrosion process. Consequently, the goal of this research was to relate inhibitor alkyl tail length to changes in activation energy of the electrochemical process associated with CO_2 corrosion of an API-5L-X65 steel at pH 4.0. Four different model compounds were synthesized in-house, and utilized to achieve this goal. Their molecular structures had the same head group, dimethylbenzylammonium, with four different alkyl tail lengths corresponding to butyl ($-C_4H_9$), octyl ($-C_8H_{17}$), dodecyl ($-C_{12}H_{25}$) and hexadecyl ($-C_{16}H_{33}$). In data analysis, the chemical component of the total activation energy was calculated using an Arrhenius-type relationship and by working at the potential of zero charge (PZC), even if this does entirely eliminate the contribution of the electrical component. A linear relationship between the tail length of the corrosion inhibitor and the change in activation energy of the corrosion process was determined, suggesting that the tail directly affects the chemical component of the total activation energy.

Key words: corrosion inhibitors, alkyl tail length, mitigation, activation energy, CO_2 corrosion

INTRODUCTION

Internal pipeline corrosion is one of the most challenging integrity problems, for management of production and transportation assets, in the oil and gas industry.[1] The associated risks have led to corrosion engineers developing both direct and indirect strategies to mitigate internal corrosion of pipelines. Injection of corrosion inhibitors is one of the most extensively applied and affordable practices to mitigate internal corrosion.[1,2]

A corrosion inhibitor is a chemical substance that can significantly reduce corrosion, in certain environments, when added in small concentrations.[3] The oil and gas industry uses a variety of corrosion inhibitors,[3] with most of them being organic surfactant-type compounds such as amines, amides and

imidazolines, which primarily function by adsorbing on the metal surface and forming a "barrier" against corrosion.[2,3] Corrosion inhibitor molecules attach to the metal surface *via* their polar (hydrophilic) head group,[4] while the non-polar, hydrophobic alkyl tail of the inhibitor is assumed to be oriented away from the surface.[4] Regarding the effect of the alkyl tail length of the corrosion inhibitors, there have been studies relating the alkyl tail with the mitigation efficiency of the corrosion inhibitors.[4–8] In those studies, corrosion efficiency and/or changes in the double layer capacitances were measured. Measurements were integrated into mathematical models based upon adsorption isotherms assuming that the coverage of the inhibitor on the metal surface (θ) is proportional to the corrosion mitigation efficiency.[3,9–11] In general, it was concluded that the longer the corrosion inhibitor alkyl tail, the greater the corrosion mitigation efficiency. However, the key link between inhibitor alkyl tail length and surface coverage is not properly established. Questions as to how a corrosion inhibitor diminishes corrosion, including establishing the mechanistic role the alkyl tail plays on the processes underlying corrosion, are not fully answered.

The most commonly accepted models to describe the retardation of the corrosion rate by a corrosion inhibitor have been based on coverage/blockage of actively corroding sites on the metal surface.[9–11] Although widely used, the idea of selective coverage of the anodic and cathodic areas implies a preferential adsorption of the inhibitor on the same electrode surface, being at odds with most widely accepted models of adsorption (e.g. the Langmuir, Frumkin, Temkin, etc.); these assume equal probability of adsorbate on any free space on the substrate, *i.e.*, uniform adsorption.[2] In order to clarify this apparent contradiction, other studies have suggested that a corrosion inhibitor might change the activation energy of either the anodic or the cathodic reaction.[12,13] However, the lack of a uniformly accepted model of inhibition and deficiencies in experimental methodologies are noticeable, even when the same type of corrosion inhibitor is used in a similar environment. For example, quaternary ammonium-type corrosion inhibitors in acidic conditions have been defined by various researchers to have "anodic"[14,15] mitigation properties, whereas other researchers claim that the same type of inhibitor exhibits "uniform"[3,16,17] inhibition properties. Consequently, the main purpose of this research is to propose a more coherent model that better describes the inhibition process and accounts for the effect of the alkyl tail length. Before continuing to the experimental part of the present study and the proposed model of corrosion inhibition, it is advisable to discuss in more detail some features and limitations of the models available in the open literature.

Model of Corrosion Inhibition Based on the Concept of Surface Coverage

This model can also be found in the literature named as the "geometrical blocking effect."[3,10,11] The idea is that the coverage by the corrosion inhibitor (θ) diminishes the actively corroding surface area of a metal by "blocking". This usually implies that the fraction of the area covered/blocked by the corrosion inhibitor does not corrode while the exposed area corrodes as if the inhibitor was not present.[9,14] Thereby, the coverage of a corrosion inhibitor can be equated to the mitigation efficiency[1–3] (η) as shown in Equation (1) and illustrated in Figure 1.

$$\theta = \eta = 1 - \frac{CR_{inhibited}}{CR_{uninhibited}} \quad (1)$$

Where $CR_{uninhibited}$ is the steady-state corrosion rate of a metal surface under specific environmental conditions without inhibitor and $CR_{inhibited}$ is the steady-state corrosion rate of a similar metal surface at the same conditions in the presence of a corrosion inhibitor.

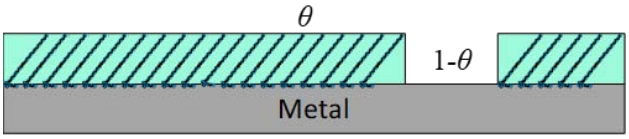

Figure 1: Interpretation of the model based on coverage. The exposed area of the metal (1-θ) corrodes as if the inhibitor is not present (usually referred to as "active area"[10,11,18]), while the area covered by the inhibitor (θ) does not corrode.

Despite being widely accepted and extensively used, advances in technology such as atomic force microscopy (AFM) and more advanced electrochemical measurements have challenged the model of corrosion inhibition based on coverage. The principal issue when mechanistically defining the surface coverage factor (θ) is the idea that the mitigation efficiency of a corrosion inhibitor depends on the extent of its adsorption.[3,10,11] Such an argument implies that a corrosion inhibitor with a high mitigation efficiency would cover the metal surface almost completely. Recent studies of corrosion inhibitors, which reported mitigation efficiencies between 80 and 90%, used atomic force microscopy (AFM) to obtain nanometer resolution images of the inhibitor on the metal surface. The AFM images show that the organic corrosion inhibitors formed a uniform and continuous film with no obvious areas that could be related to a surface coverage loss of 10% to 20%.[19–21]Even if one accounts for the concept of so called "dynamic" coverage, it is difficult to reconcile this fact with the partial surface coverage model of inhibition.

The second mechanistic issue is related to the assumption that surface coverage leads to a retardation of all electrochemical reactions underlying corrosion proportionally. Nevertheless, experimental potentiodynamic polarization curves[17] have repeatedly shown that, while affecting the charge transfer reactions, the adsorption of a corrosion inhibitor does not affect the limiting current, as shown in Figure 2. If there were a true reduction of "active surface area" the limiting current would also be diminished by the presence of a corrosion inhibitor.

There are other questions that could be raised about the models of inhibition based solely on the concept of coverage/blockage, which cannot be readily answered, particularly those related to so called selective adsorption, but this discussion exceeds the scope of the present paper.

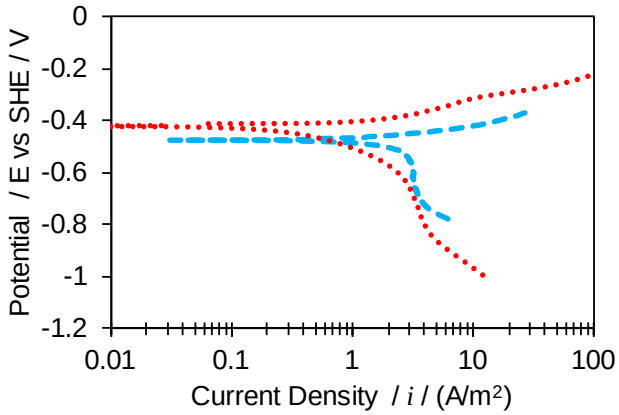

Figure 2. Experimental potentiodynamic sweeps on a mild steel RCE in CO_2 purged 1 wt. % NaCl electrolyte at pH 4, 30°C, 1000 RPM. Dashed blue line: no inhibitor. Dotted red line: 110 ppm quaternary ammonium chloride-based corrosion inhibitor. The limiting current remains unaffected despite the presence of a corrosion inhibitor.

Model of Inhibition Based on Change of Overall Activation Energy for the Corrosion Process

In some studies it was suggested that the adsorption of a corrosion inhibitor can be best qualified by the effect it has on the overall activation energy for the corrosion process,[11–13] which is a measure of the

associated kinetics. In order to determine the overall activation energy of corrosion processes an Arrhenius-type equation has been used in the past,[11–13] as shown in Equation (2).

$$i_{corr} = A\exp\left(-\frac{\Delta G_M^*}{RT}\right) \quad (2)$$

Where: ΔG_M^* is the overall activation energy for the corrosion process, A is a pre-exponential factor, R is the ideal gas constant, and T is the absolute temperature.

Whilst this is a theoretically valid approach, the problem with calculating the overall activation energy for the corrosion process does not properly account for the fact that, during corrosion, at least two distinct reactions proceed at the same rate: cathodic (in the present case of corrosion of mild steel in acidic environments, reduction of hydrogen ion) and anodic (here oxidative iron dissolution).[2,22-23] Therefore, the overall activation energy for the corrosion process is some composite measure of the activation energies of the dominant cathodic and anodic reaction, which can be quite different. The situation is further complicated by the fact that for acidic environments, the cathodic hydrogen ion reduction reaction can be under charge transfer, mass transfer, chemical reaction rate or mixed control, each having distinct kinetics and activation energies. Therefore, having a single measure of the kinetics in the form of an overall activation energy for the corrosion process, without considering the abovementioned mechanistic distinctions, yields results that cannot be readily generalized. Consequently, this approach has produced widely dispersed values for the overall activation energy for the corrosion process,[11–13] ranging from 10 to 60 kJ mol^{-1}.

Model of Inhibition Based on Change of Electrochemical Activation Energy for the Individual Reactions Underlying the Corrosion Process

A more effective approach is to try and look at the activation energy (kinetics) of individual anodic and cathodic reactions underlying the corrosion process. Given that these are electrochemical reactions, they involve charged ionic species moving across an electric field generated by a double layer structure at the metal surface. Therefore, in a general case, one needs to consider both the chemical and the electrical component of the activation energy.[24–26] Figure 3 presents a sketch, illustrating a textbook example[24] of the oxidative dissolution of a metal and the associated free energy diagram, showing the total activation energy for this reaction as being composed of two parts; a chemical component and an electrical component:

$$\Delta\tilde{G}_M^* = \Delta G_M^* + \beta F\Delta\Phi \quad (3)$$

where $\Delta\tilde{G}_M^*$ is the total activation free energy, ΔG_M^* is the chemical component of the activation energy of the electrochemical process, β is a symmetry factor, F is the Faraday constant and $\Delta\Phi$ is the potential drop across the double layer.

For the case of inhibition, one can use this approach to look at the effect of inhibitor adsorption on the activation energy change of individual reactions underlying corrosion, and then make a distinction between the effect the adsorbed inhibitor layer has on the chemical and electrical component of the total activation energy of that reaction. The text below illustrates how this can be done, with the practical example considered being the effect of the alkyl tail length of the corrosion inhibitors on inhibition efficiency.

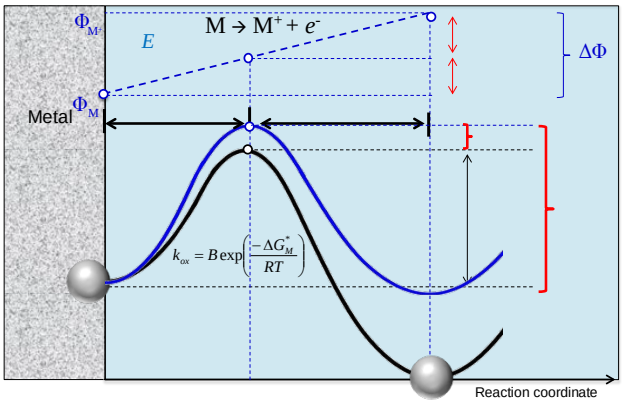

Figure 3. Representation of the free energy diagram for an anodic reaction ($M \rightarrow M^+ + e^-$). The total activation energy of this reaction is divided into chemical component (black curve) and electrical component (dashed blue line). The combination of the two is shown as a solid blue curve. Adapted from Bockris, *et al.* [24]

EXPERIMENTAL PROCEDURE

Synthesis of Corrosion Inhibitor Model Compounds

In order to be able to effectively isolate the effect of the alkyl tail length of the corrosion inhibitors, four different model compounds were synthesized in-house and tested against CO_2 corrosion of mild steel. The model compounds consisted of the same head group, dimethyl-benzyl-ammonium, with four different alkyl tail lengths: butyl ($-C_4H_9$), octyl ($-C_8H_{17}$), dodecyl ($-C_{12}H_{25}$) and hexadecyl ($-C_{16}H_{33}$). The general synthesis reaction is as depicted in

Figure 4.

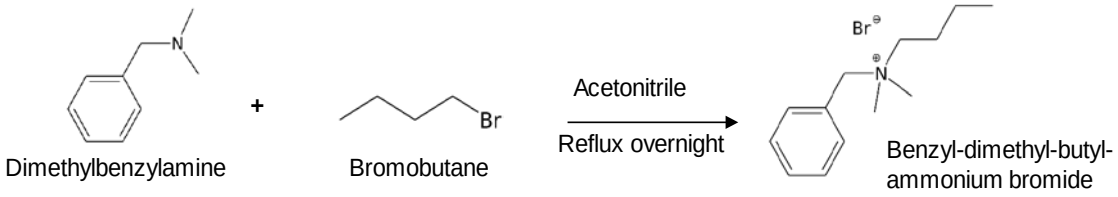

Figure 4: General reaction for the model compounds utilized as corrosion inhibitors.

The chemical structure for each model compound is given in Table 1. The model compounds in this work are named according to the number of carbon atoms in the alkyl tail. The "Q" stands for quaternary ammonium compound.

Table 1
Chemical Structure of Model Compounds.

Compound	Name
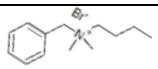	Q-C4
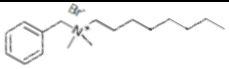	Q-C8
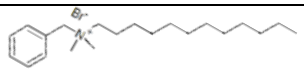	Q-C12
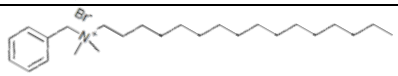	Q-C16

Proton nuclear magnetic resonance (^{1}H-NMR or simply NMR) spectroscopy was used to characterize the synthesized model compounds, corroborating their theoretical chemical structure and assessing their purity. Each individual peak of the spectra was numerically integrated. The integration gave the number of hydrogen atoms measured in each peak related to its molecular position. Figure 5 shows the NMR spectra for all the synthesized corrosion inhibitor model compounds. The spectra showed a good agreement with the expected structure. Moreover, peaks unrelated to the structure were numerically integrated to determine the level of impurities, which are negligible (*ca.* 99% of purity).

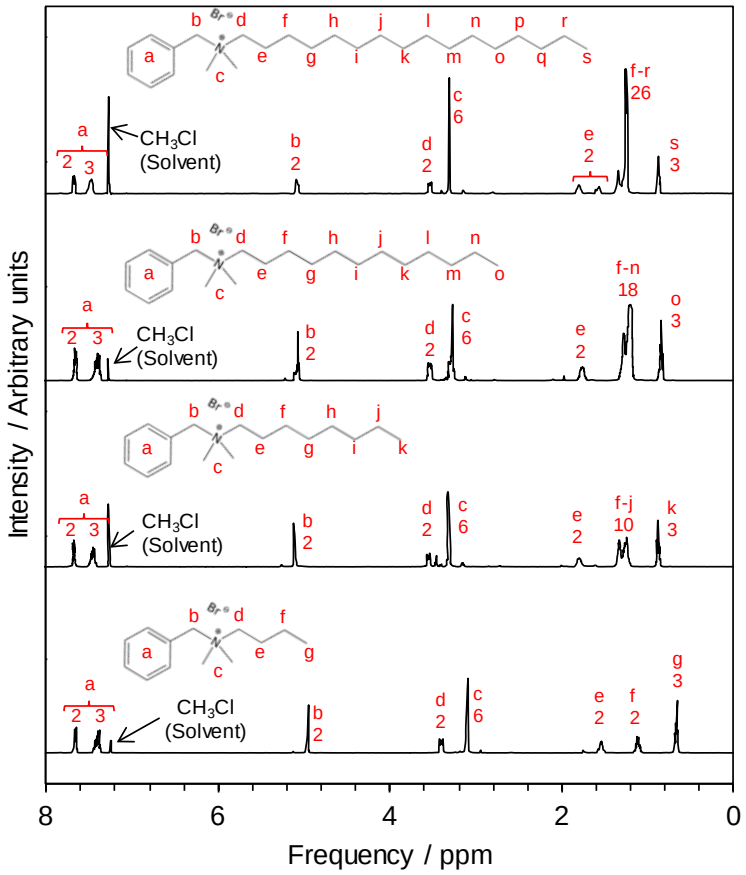

Figure 5: Proton NMR for Q-C16, Q-C12, Q-C8, Q-C4. Letters in each peak indicates the number of hydrogen atoms obtained from integration. The letters are associated with the theoretical structure of the model compound.

Electrochemical Experiments

A three-electrode glass cell setup was used to perform corrosion and corrosion mitigation experiments at 1 bar, pH 4 and 30, 35, 40 and 45 °C with a 1 wt % NaCl solution; an UNS K03014 API 5L X65[27] steel rotating cylinder electrode (RCE) at 1000 rpm was used as the working electrode as shown in

Figure 6. The composition of the steel is shown in Table 2. A platinum covered titanium mesh was used as a counter electrode and an Ag/AgCl (KCl saturated) reference electrode was used as the reference. CO_2 was used for purging the system and the solution pH was adjusted and maintained at pH 4.0±0.1 during each experiment. Linear polarization resistance (LPR) measurements were taken to obtain the charge transfer resistance by polarizing the working electrode ±5 mV from the corrosion potential; corrosion rates were then calculated by using a *B* value of 26 mV/decade. Electrochemical impedance spectroscopy (EIS) was used for measuring solution resistance using an oscillating potential ±5 mV with

respect to the corrosion potential. Each experiment was performed three times. A summary of the experimental conditions is given in

Table 3.

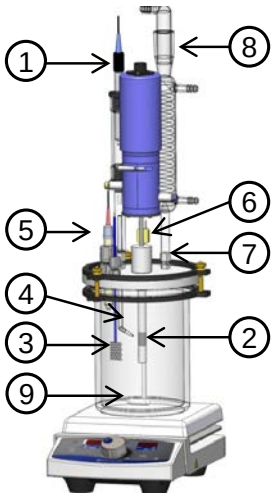

1. Reference Electrode (RE – Saturated Ag / AgCl)
2. Rotating Cylinder Electrode (WE)
3. Counter Electrode (CE)
4. Luggin Capillary
5. pH Meter
6. Thermocouple
7. Gas in
8. Gas out
9. Magnetic Stirrer

Figure 6: Three electrode set up used to perform experiments.[(1)]

Table 2
Chemical Composition of the X65 Steel Used as Working Electrode

Composition	Elements									
	Cr	Mo	S	V	Si	C	Ni	Mn	P	Fe
Weight %	0.14	0.16	0.009	0.047	0.26	0.13	0.36	1.16	0.009	Balance

Table 3
Experimental Conditions

Description	**Parameters**
Test material	API 5L X65
Working solution	1 wt.% NaCl
Sparge gas	CO_2
Temperature / ˚C	30, 35, 40, 45
pH	4.0 ± 0.1
Corrosion inhibitors	None (baseline), Model Compounds: Q-C4 (50, 100, 150, 200 ppm V/V) Q-C8 (50, 100, 150, 200 ppm V/V) Q-C12 (50, 100, 150, 200 ppm V/V) Q-C16 (50, 100, 150, 200 ppm V/V)
Test duration	2-12 hours (stabilization of corrosion rate)
Measurement methods	LPR, EIS, potentiodynamic polarization
Potentials for EIS (E vs SHE / mV)	-650, -550, -500, -450, -400, -350, -300

[(1)] Image courtesy of Cody Shafer, ICMT, Ohio University.

RESULTS AND DISCUSSION

One of the first concepts that needed to be established in this approach is the saturation of the metal surface with an adsorbing corrosion inhibitor, which was proposed and described by Hackerman *et al.*[28] This refers to a situation where a corrosion inhibitor will keep adsorbing onto the metal surface (and the corrosion rate will keep diminishing) until the surface is saturated with the inhibitor and any further addition of the inhibitor to the bulk solution will not result in a measurable/significant increase of the amount of adsorbed inhibitor and will not lead to a further decrease of the corrosion rate.[28] That amount of added inhibitor is called the surface saturation concentration[28].

In the current study, the corrosion inhibitor concentration that produces a surface saturation was determined for each corrosion inhibitor at four different temperatures. Individual experiments were performed, starting from 50 ppm and increasing in 50 ppm increments until the corrosion rate was not significantly diminished, as illustrated in

Figure 7. The graph shows four different and independent experiments performed at 0.96 bar CO_2, pH 4.0, 30°C, and RCE set to 1000 rpm with increasing concentration of the model compound Q-C12. In this case, the minimum concentration of the inhibitor that yielded a minimum corrosion rate was estimated to be 100 ppm. A similar series of experiments was performed for each inhibitor. The results are summarized in Table 4. The surface saturation concentration was observed to diminish proportionally to the increase in alkyl tail length.

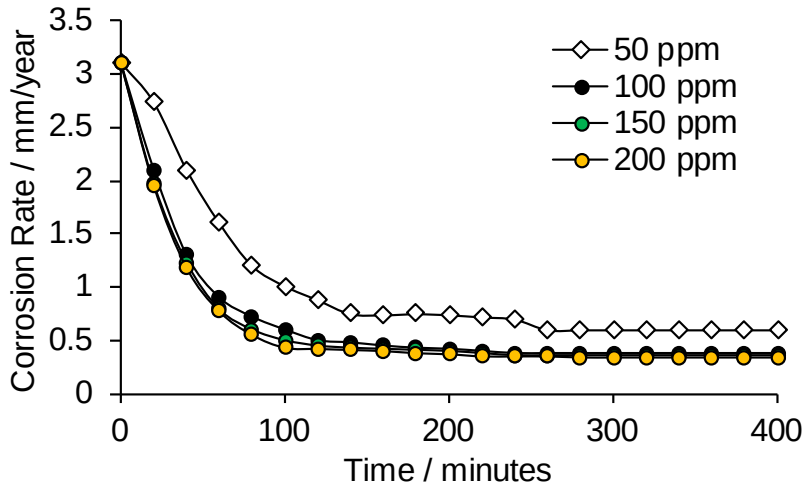

Figure 7: Approach to find the lowest concentration of corrosion inhibitor to attain the maximum efficiency. In the graph: Q-C12 model compound in four independent tests at 0.96 bar CO_2, pH 4, 30°C, RCE at 1000 rpm.

Table 4
Surface Saturation Concentration of Corrosion Inhibitors

Compound	Surface Saturation Concentration / ppm (V/V)
Q-C4	200
Q-C8	150
Q-C12	100
Q-C16	50

At the outset, it was assumed that at surface saturation concentration, the adsorbed organic inhibitor forms a uniform film that affects both components of the electrochemical activation energy: the chemical

and the electrical component. In an attempt to separate the two, the chemical activation energies were found at the potential of zero charge (PZC). This was done based on an assumption that the electrical component of the activation energy was minimized at the PZC, so that the rate constant of the process obtained *via* an Arrhenius plot was dominated by the chemical component. It was also assumed that the corrosion rate was inversely proportional to the polarization resistance (according to the Stern-Geary equation[29,30]). The PZC was found *via* the minimum capacitance method[31] using a typical three-electrode RCE glass cell, at 1000 rpm. EIS measurements were potentiostatically taken at applied potentials (as shown in Table 3 between -0.85 and -0.5 V (vs. saturated Ag/AgCl) using a frequency range between 10 mHz to 5 kHz. Effective double layer capacitances were obtained by the method formulated by Tribollet *et al.,* described elsewhere[32].

The results for the determination of the PZC for pH 4.0, 0.96 bar CO_2, 1 wt.% NaCl, 30°C electrolytes with and without the presence of the corrosion inhibitor model compounds are shown in Figure 8. As can be seen, after the addition of the model compounds at their respective surface saturation concentrations, the capacitance decreased proportionally with the increase of the inhibitor alkyl tail length. In the presence of the inhibitor, it can be observed that there is no dependence of capacitance on the applied potential (since horizontal regression lines are within the error bars of measurements) and, consequently, there was no clear potential of zero charge. This is presumably because after being adsorbed onto the metal surface, the organic model compounds were unresponsive to a change in the electric field[31,33] within the range of potentials tested here. It can also be noticed from Figure 8 that the open circuit potential (OCP) in the absence of inhibitor is negative with respect to the PZC. This condition indicates that the freely corroding steel surface was “negatively charged”[33]. Thereby, the adsorption of cationic species, such as the model inhibitor compounds, was promoted. Figure 9 shows that the decrease in capacitance is correlated to the decrease of corrosion rate. Both effects are proportional to the alkyl tail length. This can be explained by the changes in the relative permittivity, also known as the dielectric constant (ε_r) within the double layer, due to the presence of an adsorbed organic substance[33]. As a secondary effect, the OCP in the presence of corrosion inhibitors changed towards a more positive potential. This effect can be explained by changes of the cathodic reaction from mixed/mass transfer control to charge transfer control. Details of this effect are provided elsewhere.[17]

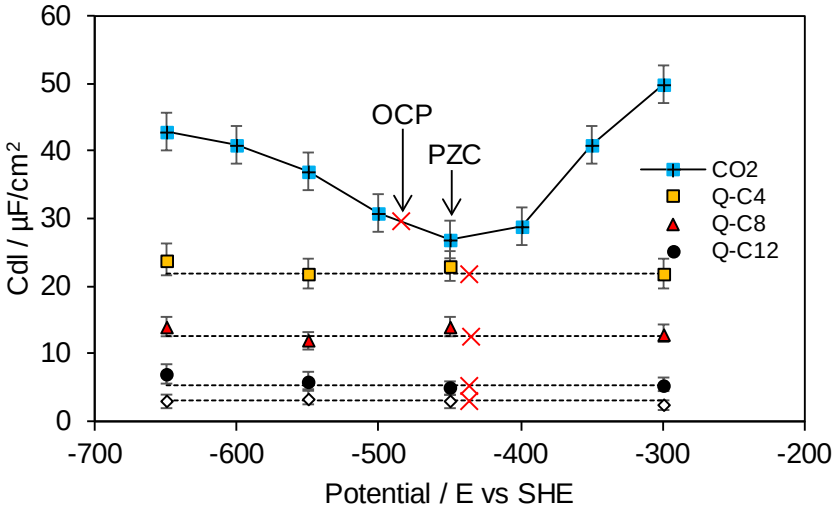

Figure 8: Capacitance *versus* potential. RCE at 1000 rpm in a pH 4.0, 0.96 bar CO_2, 1 wt.% NaCl, 30°C solution with and without the presence of the corrosion inhibitors model compounds at their respective surface saturation concentration. Open circuit potential (OCP) indicated with the red cross. PZC indicated for the system without model compounds.

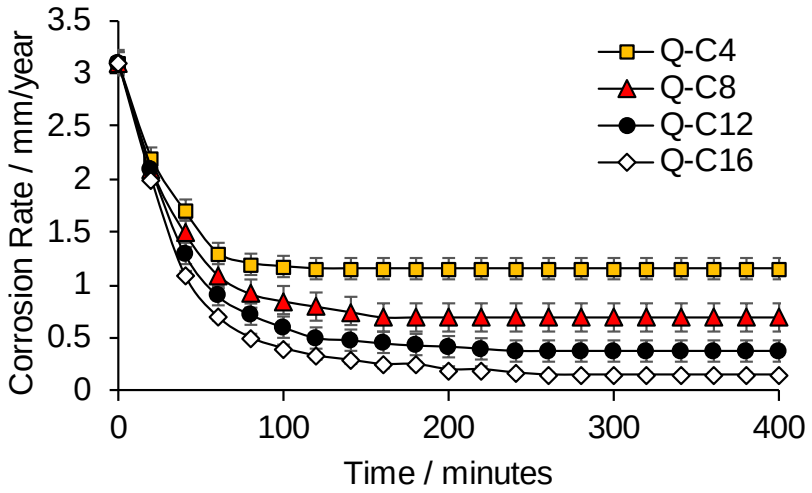

Figure 9: Corrosion rates with time as a function of the synthesized model compounds added at their respective surface saturation concentration. RCE at 1000 rpm in a pH 4.0, 0.96 bar CO_2, 1 wt. % NaCl, 30°C

Theoretically, the chemical component of the total activation energy in the electrochemical dissolution of a metal can be thought as the activation energy of the metal dissolution in the absence of the electrical double layer effect. In this scenario, the water molecules help ionize/reorganize the metal atoms as they cross the energy barrier previously depicted in Figure 3. It can also be seen as the effect of water on the so called "reorganization energy", as described in the literature.[22,34,35] The adsorbed corrosion inhibitor alters the ionization energy of metal atoms as they dissolve in water, by displacing water molecules from the metal surface and making the ionization of the metal ions more difficult. Consequently, the chemical component of the activation energy relating to metal dissolution increases. Figure 10 qualitatively illustrates such a change.

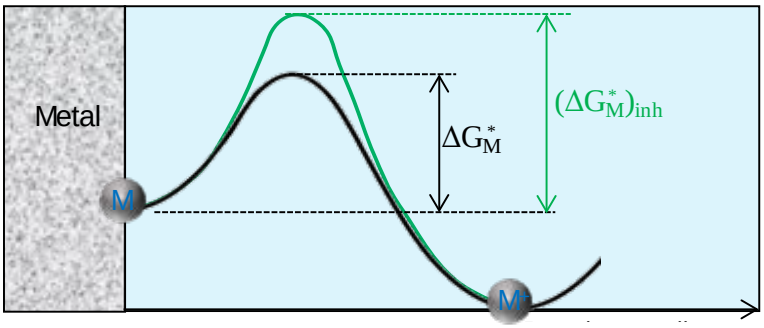

Figure 10: Increase of the chemical component of the activation energy. ΔG_M^* is the activation energy without inhibitor and $(\Delta G_M^*)_{inh}$ is the activation energy in the presence of a corrosion inhibitor.

In order to determine the chemical contribution of the total activation energy, experiments were conducted at the potential of zero charge (PZC) in order to minimize the contribution of the electrical field (it is practically impossible to totally eliminate it in a way that would be theoretically desirable). The activation energy associated with the corrosion process was determined *via* an Arrhenius plot. The polarization resistances were taken from the Nyquist plot of the impedance measured at the PZC at different temperatures. As shown in Figure 11, no changes in the PZC were detected in the used temperature range.

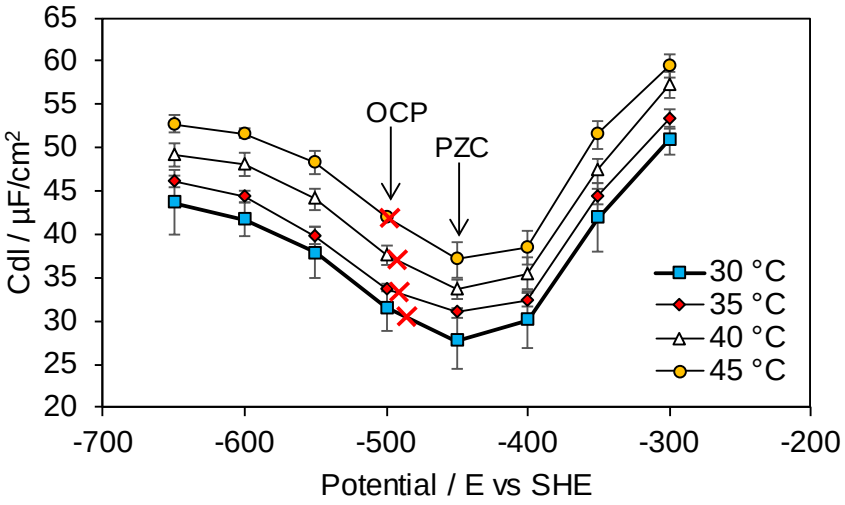

Figure 11: Capacitance *versus* potential. RCE at 1000 rpm in a pH 4.0, 0.96 bar CO_2, 1 wt. % NaCl, at different temperatures. PZC indicated with the arrow. OCP indicated with the red cross.

As explained above, it was here assumed that the rate constant of the iron dissolution was dominated by the chemical component of the activation energy. The logarithm of the polarization resistance was plotted *versus* the inverse of the absolute temperature. Figure 12 shows the Arrhenius plot for a CO_2 system with no corrosion inhibitor. The activation energy was determined to be *ca.* 47 kJ mol^{-1}. Since the PZC where the measurements were taken was 30-50 mV more positive than the open circuit potential in the presence of the inhibitor (as seen in Figure 11), it can be assumed that this activation energy refers to the dominant reaction, which is in this case the anodic dissolution of iron. It is well established in CO_2 corrosion of mild steel that this reaction is under charge transfer control,[14] as can be gathered from Figure 2.

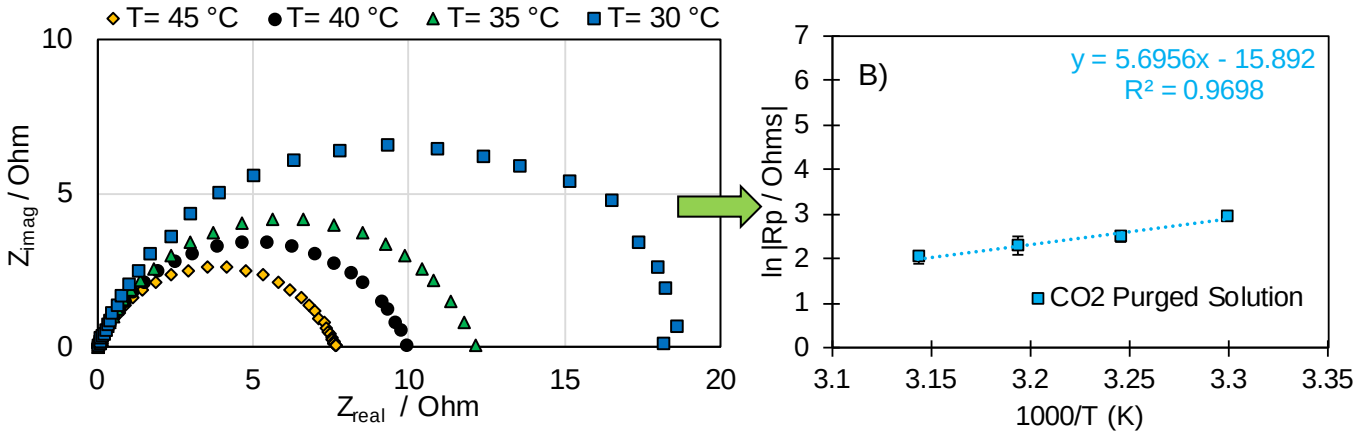

Figure 12: Determination of activation energy *via* an Arrhenius plot in a CO_2 system with no corrosion inhibitor. A) Nyquist plot for a CO_2 system with no corrosion inhibitor at four different temperatures. Measurements taken at PZC. The ohmic solution resistance was compensated for. B) Activation energy was calculated to be 46.9 ± 1.8 kJ mol^{-1}

Since no clear PZC was detected in the presence of corrosion inhibitors, the activation energy in all experiments was determined at the PZC found in the absence of corrosion inhibitors (-450 mV *vs.* SHE), in order to compare the changes in activation energy, similarly to the method proposed by Gileadi, *et al.*[36] The addition of a corrosion inhibitor increased the activation energy of the iron dissolution process. Figure

13 depicts obtaining the activation energy in the presence of the model compound Q-C12. The activation energy increased from 47 to *c.a.* 54 kJ mol^{-1}.

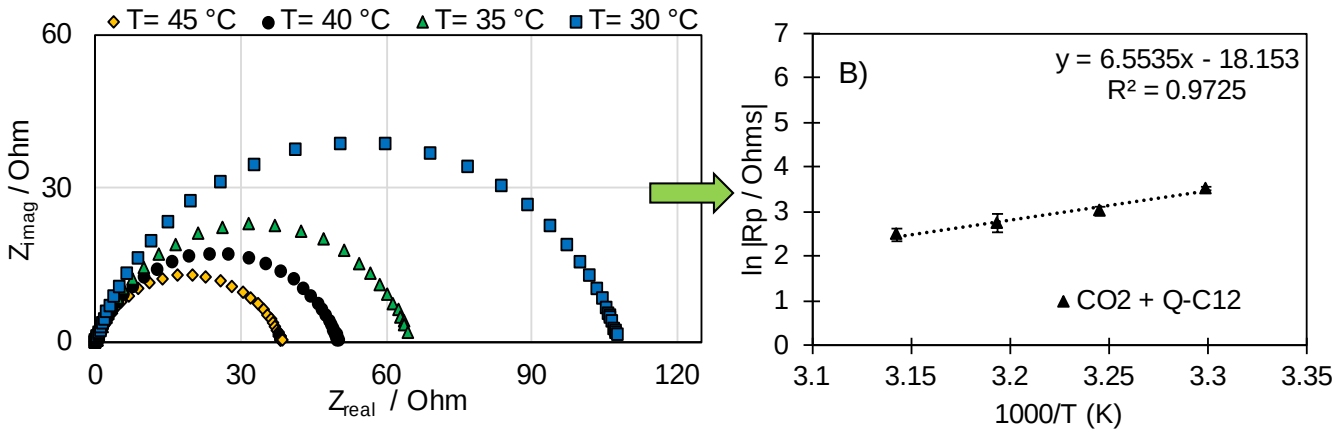

Figure 13: Determination of activation energy *via* an Arrhenius plot in a CO_2 system with corrosion inhibitor at its surface saturation concentration. A) Nyquist plot for a CO_2 system with corrosion inhibitor Q-C12 at four different temperatures. Measurements taken at the PZC of the CO_2 system (-450 mV vs. SHE). The ohmic solution resistance was compensated for. B) Activation energy was calculated to be 53.8 ± 1.5 kJ mol^{-1}.

The measured activation energies for the CO_2 corrosion process in the presence of the adsorbed corrosion inhibitor model compounds were plotted against their respective alkyl tail lengths. Advanced molecule editor software was used to visualize the structure of the synthesized model compounds and to determine the alkyl tail length in Angstroms (Å)[37]. The structures with their calculated alkyl tail lengths are shown in

Figure **14**. The plot of the activation energies *versus* model compound alkyl tail length is shown in

Figure 15. The plot shows a linear relationship between the activation energy and the increase of the inhibitor tail length. In addition, if the resulting graph is extrapolated to “zero-long” alkyl tail, the result is *ca.* 48.5 kJ mol^{-1}, which is very close to the activation energy in the absence of corrosion inhibitors (47 kJ mol^{-1}). This result suggests that the role of the head group in the quaternary ammonium compound is primarily to attach to the metal surface and the alkyl tail length is responsible for modifying the chemical activation energy of the electrochemical process underlying CO_2 corrosion. The observed increase in activation energy can plainly be interpreted by the hydrophobicity of the non-polar inhibitor alkyl tail, which repels water more effectively when its length increases. Due to the dilution/displacement of water by the adsorbed inhibitor molecules at the metal surface, the ionization activation energy of the metal increases and, as a result, the anodic dissolution of iron proceeds at a lower rate.

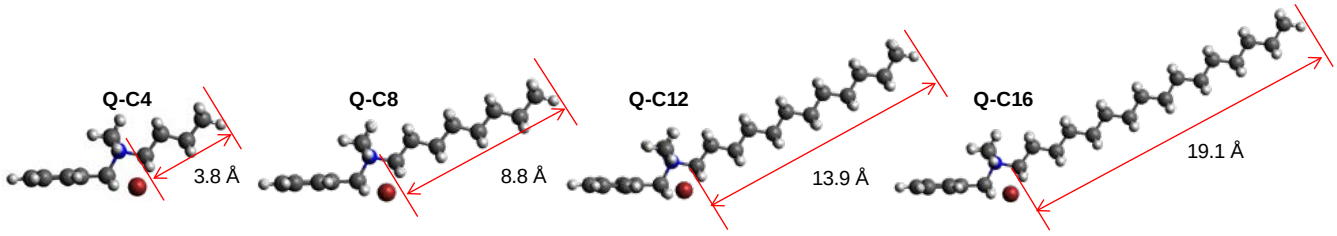

Figure 14: Structure and calculated alkyl tail lengths of the synthesized model compounds.

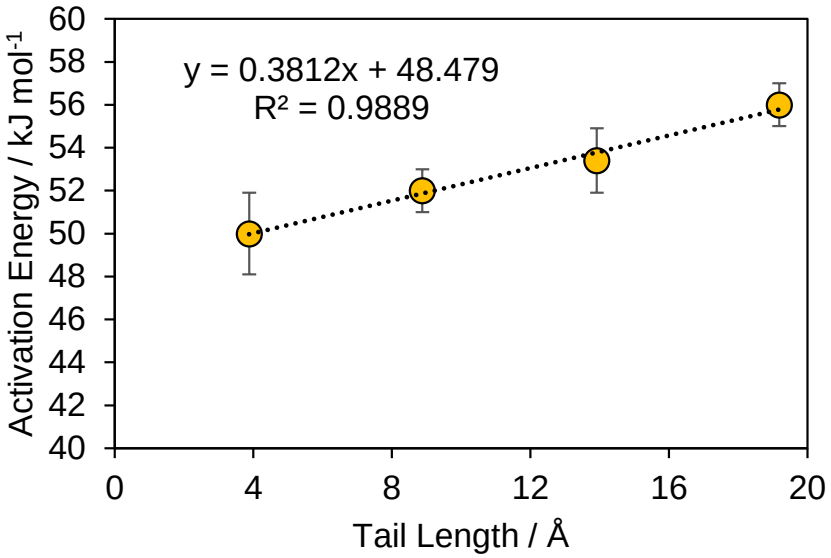

Figure 15: Activation energies of inhibited CO_2 corrosion *versus* inhibitor alkyl tail length. Error bars: maximum and minimum values obtained from three performed experiments at each point.

CONCLUSIONS

- The surface saturation concentration was determined for each model corrosion inhibitor, which was observed to diminish proportionally to the increase in alkyl tail length.
- Corrosion rates were measured at the critical surface saturation concentration for each inhibitor. Results indicated that the longer the alkyl tail length, the greater the corrosion mitigation efficiency for the homologous series evaluated.
- The activation energies for each inhibitor were obtained at their respective surface saturation concentration. The longer the tail, the larger the increase in activation energy.
- Results suggest that the main role of the head group of the quaternary ammonium model compounds is to help attach the inhibitor molecule to the metal surface, while the hydrophobicity of the alkyl tail plays a governing role in the inhibition process by displacing water molecules from the surface and increasing the chemical activation (ionization energy) for metal dissolution.

ACKNOWLEDGMENTS

The authors would like to thank the following companies for their financial support: Anadarko, Baker Hughes, BP, Chevron, CNOOC, ConocoPhillips, DNV GL, ExxonMobil, M-I SWACO (Schlumberger), Multi-Chem (Halliburton), Occidental Oil Company, Petrobras, PTT, Saudi Aramco, Shell Global Solutions, SINOPEC (China Petroleum), TransCanada, TOTAL, and Wood Group Kenny.

The authors also express their gratitude to Dr. Andrew Tangonan and the Chemistry & Biochemistry Department at Ohio University for their assistance in collecting NMR data.

REFERENCES

1. D. A. Jones, *Principles and prevention of corrosion*, 2nd ed. (New York, NY: MacMillan, 1996), pp. 503-570.
2. E. McCafferty, *Introduction to corrosion science*, (New York, NY: Springer, 2010), pp. 359-400.
3. V. S. Sastri, *Green Corrosion Inhibitors*, 2nd ed. (Hoboken, NJ: John Wiley & Sons, 2011), p. 110.
4. A. Edwards, C. Osborne, S. Webster, D. Klenerman, M. Joseph, P. Ostovar, and M. Doyle, "Mechanistic studies of the corrosion inhibitor oleic imidazoline," *Corrosion Science* 36, 2, (1994): pp. 315–325.
5. M. Palomar-Pardavé, M. Romero-Romo, H. Herrera-Hernández, M.A. Abreu-Quijano, N. V. Likhanova, J. Uruchurtu, and J.M. Juárez-García, "Influence of the alkyl chain length of 2 amino 5 alkyl 1,3,4 thiadiazole compounds on the corrosion inhibition of steel immersed in sulfuric acid solutions," *Corrosion Science* 54, 1, (2012): pp. 231–243.
6. D. Asefi, M. Arami, A.A. Sarabi, and N.M. Mahmoodi, "The chain length influence of cationic surfactant and role of nonionic co-surfactants on controlling the corrosion rate of steel in acidic media," *Corrosion Science* 51, 8, (2009): pp. 1817–1821.
7. S. A. Ali, A.M. El-Shareef, R.F. Al-Ghamdi, and M.T. Saeed, "The isoxazolidines: The effects of steric factor and hydrophobic chain length on the corrosion inhibition of mild steel in acidic medium," *Corrosion Science* 47, 11, (2005): pp. 2659–2678.
8. E. McCafferty and N. Hackerman, "Double layer capacitance of iron and corrosion inhibition with polymethylene diamines," *Journal of the Electrochemical Society* 119, 2, (1972): pp. 146-154.
9. L. M. Vracar and D. Drazic, "Adsorption and corrosion inhibitive properties of some organic molecules on iron electrode in sulfuric acid," *Corrosion Science* 44, (2002): pp. 1669–1680.
10. W. J. Lorenz and F. Mansfeld, "Interface and interphase corrosion inhibition," *Electrochimica Acta* 31, 4, (1985): pp. 467–476.
11. C. Cao, "On electrochemical techniques for interface inhibitor research," *Corrosion Science* 38, 12, (1996): pp. 2073–2082.
12. Y. Zhu, M. L. Free, and G. Yi, "The effects of surfactant concentration, adsorption, aggregation, and solution conditions on steel corrosion inhibition and associated modeling in aqueous media," *Corrosion Science* 102, (2016): pp. 233–250.
13. G. Zhang, C. Chen, M. Lu, C. Chai, and Y. Wu, "Evaluation of inhibition efficiency of an imidazoline derivative in CO_2 -containing aqueous solution," *Materials Chemistry Physics* 105, 2, (2007): pp. 331–340.
14. S. Nešić, W. Wilhelmsen, S. Skjerve, and S.. M. Hesjevik, "Testing of inhibitors for CO_2 corrosion using the electrochemical techniques," *Proceedings of the 8th European Symposium on Corrosion Inhibitors* 10, (1995): pp. 1163–1192.
15. R. Zvauya and J. L. Dawson, "Inhibition studies in sweet corrosion systems by a quaternary ammonium compound," *Journal of Applied Electrochemistry* 24, 9, (1994): pp. 943–947.
16. K. Bílková and E. Gulbrandsen, "Kinetic and mechanistic study of CO_2 corrosion inhibition by cetyl trimethyl ammonium bromide," *Electrochimica Acta* 53, 16, (2008): pp. 5423–5433.
17. J. M. Dominguez Olivo, B. Brown, and S. Nesic, "Modeling of corrosion mechanisms in the presence of quaternary ammonium chloride and imidazoline corrosion inhibitors," NACE Corrosion Conference 2016, paper 7406 (Houston, TX: NACE, 2016).
18. D. M. Drazic, L. Vracar, and V. J. Drazic, "Kinetics of inhibitor adsorption on iron," *Electrochimica Acta* 39, 8, (1994): pp. 1165–1170.
19. V. Pandarinathan, K. Lepkova, S.I. Bailey, T. Becker, and R. Gubner, "Adsorption of corrosion inhibitor 1‑dodecylpyridinium chloride on carbon steel studied by in situ AFM and electrochemical methods," *Industrial & Engineering Chemistry Research* 53, (2014) pp. 5858–5965.

20. O. Olivares-Xometl, O., N.V. Likhanova, M. A. Domínguez-Aguilar, J.M. Hallen, L.S. Zamudio, and E. Arce, “Surface analysis of inhibitor films formed by imidazolines and amides on mild steel in an acidic environment,” *Applied Surface Science* 252, 6, (2006): pp. 2139–2152.
21. B. Wang, M. Du, J. Zhang, and C.J. Gao, “Electrochemical and surface analysis studies on corrosion inhibition of Q235 steel by imidazoline derivative against CO2 corrosion,” *Corrosion Science* 53, 1, (2011): pp. 353–361.
22. A. Bard and L. Faulkner, *Electrochemical Methods Fundamentals and Applications*, 2nd ed. (New York, NY: John Wiley & Sons, Inc., 2001).
23. J. O. Bockris, D. Drazic, and A. Despic, “The electrode kinetics of the deposition and dissolution of iron,” *Electrochimica Acta* 4, (1961): pp. 325-361.
24. J. O. Bockris, A. K. N. Reddy, and M. Gamboa-Adelco, *Modern Electrochemistry 2A, Fundamentals of Electrodics*, (New York, NY: Springer, 2001), pp. 1–817.
25. J. O. Bockris and Z. Nagy, “Symmetry factor and transfer coefficient. A source of confusion in electrode kinetics,” Journal of Chemical Education 50, 12, (1973): pp. 839-843.
26. F. K. Crundwell, “The dissolution and leaching of minerals: Mechanisms, myths and misunderstandings,” *Hydrometallurgy* 139, (July 2013): pp. 132–148.
27. API 5L (latest revision), “Specification for Line Pipe” (Washington, DC: American Petroleum Institute).
28. T. Murakawa, S. Nagaura, and N. Hackerman, “Coverage of iron surface by organic compounds and anions in acid solutions,” *Corrosion Science* 7, 2, (1967): pp. 79–89.
29. M. Stern, “Electrochemical Polarization,” *Journal of the Electrochemical Society* 104, 9, (1957): pp. 53-63.
30. W. J. Lorenz and F. Mansfeld, “Determination of corrosion rates by electrochemical DC and AC methods,” *Corrosion Science* 21, 9, (1981): pp. 647–672.
31. P. Delahay, *Double layer and electrode kinetics*, (New York, NY: John Wiley and Sons, Inc., 1965). pp. 126-142.
32. B. Hirschorn, M.E. Orazem, B. Tribollet, V. Vivier, I. Frateur, and M. Musiani, “Determination of effective capacitance and film thickness from constant-phase-element parameters,” *Electrochimica Acta* 55, 21, (2010): pp. 6218–6227.
33. Damaskin, O. A. Petrii, and V. Batrakov, *Adsorption of organic compounds on electrodes*, (New York, NY: Plenum Press, 1971).
34. S. Fletcher, “The theory of electron transfer,” *Journal of Solid State Electrochemistry* 14, 5, (February 2010): pp. 705–739.
35. R. A. Marcus, “On the theory of electron-transfer reactions. VI. Unified treatment for homogeneous and electrode reactions,” *The Journal of Chemical Physics* 43, 2 (1989): pp. 679-701.
36. E. Gileadi, *Electrosorption*, 1st ed. (New York, NY: Plenum Press, 1967), pp. 87-114.
37. M. D. Hanwell, D.E. Curtis, D.C. Lonie, T. Vandermeerschd, E. Zurek, and G.R. Hutchison, “Avogadro: An advanced semantic chemical editor, visualization, and analysis platform,” *Journal of Cheminformatics* 4, 17, (2012): p 113.